Transition from Sleeve Bearings to AMBs in 1 MW High-Speed Motor for Turbomachinery – Lessons Learned –

Robert SEIFERT*, Sebastian VETTER*, Andreas GÜNDEL*, Alexander SMIRNOV** and Jens PROSKE*
* VEM Sachsenwerk GmbH
Pirnaer Landstraße 176, 01257 Dresden, Germany
E-mail: robert.seifert@vem-group.com
** SpinDrive Oy
Laserkatu 6, 53850 Lappeenranta, Finland

Abstract
We present a 1 MW high–speed motor featuring a levitating rotor supported by active magnetic bearings (AMBs), addressing an expected growing market demand for oil–free and gearless drives for high–speed turbomachinery. Our internally developed bearing concept leverages our extensive experiences in the field of electrical high–voltage machines, revealing both synergies as well as novel challenges. This article focuses on the *lessons learned* during the design, manufacturing, and commissioning of these AMBs. We discuss the critical physical boundaries influencing material selection and the trade–offs necessary for manufacturability and the consistency of elements like interference fits. A test run at 15 000 rpm serves as a proof-of-concept, demonstrating the reliability, stability, and vibration levels of the magnetic levitation with overall satisfactory results. However, in the frequency range below 300 Hz we still see room for improvement. Low–frequency housing modes coincide with the broadband excitation of the magnetic bearings causing higher–than–expected vibration amplitudes, although still acceptable. We conclude by proposing enhancements to the bearing controller and emphasize the critical need for structural stiffening of the motor's housing and bearing shield to effectively decouple controllable rotor modes from unavoidable housing vibrations, which is essential for future performance optimization.

Keywords : turbomachinery, commissioning, controller synthesis, rotor dynamics, rotor design

1. Introduction

The oil and gas industry must constantly reduce its CO_2 emissions following the European Green Deal or US Clean Air Act, to name a few. That leads to a high demand for electric drives to substitute gas turbines in new as well as existing compressor plants and industrial heat pumps. To keep the footprint small and drivetrain short, especially for retrofits, gearless high–speed drives are preferred. Their variable frequency enables an efficient process control without the losses of the otherwise required turbo gear box or due to throttle valves. To increase acceptance for high–speed drives in a broader market, motor manufacturers are challenged to offer simple and affordable solutions. Sleeve bearings and the more specialized tilting–pad bearings are suitable for a large range of applications in this market, but oil–free active magnetic bearings (AMBs) can further reduce the environmental impact and eliminate contamination. They are maintenance–free and allow a simple condition monitoring in most compact plant installations. However, AMBs are costly and their commissioning comparatively time–consuming.

In 2022 we manufactured a first prototype with three–lobe sleeve bearings from Renk which ran between 12 000 rpm and 17 000 rpm, depending on the different rotor concepts we tested (laminated rotor with die–cast aluminium cage vs. slitted solid rotor). Starting from 14 000 rpm the sleeve bearings showed instabilities, disqualifying them from their usage at such high speeds. That is why we changed to tilting–pad bearings in subsequent comparable projects. We also developed a new prototype with a revised solid rotor concept with copper cage, designed to mechanically withstand up to 18 000 rpm, which also serves as a proof–of–concept for an oil–free alternative based on active magnetic bearings. In this article we focus on the latter prototype and give insights in the lessons we learned during the design, manufacturing and commissioning of our first in–house AMB concept for a turbo compressor drive (≈1 MW, 12 000…18 000 rpm).

Figure 1 a) High–speed prototype motors (left: sleeve bearings, right: magnetic bearings) coupled with membrane–coupling, attached control cabinet with SpinDrive Magma X800 MBC Controller for remote servicing
b) Prototype with sleeve bearings coupled with turbo compressor in SEC test field © Siemens Energy, 2024
—Siemens Energy is a trademark licensed by Siemens AG.

2. Drive Concept and Magnetic Bearing Design

In general, there are two ways to achieve a compressor drivetrain using high–speed motors as depicted in Durantay et al. (2023). For the first option the compressor (or similar load machine) remains unchanged and is coupled directly to the standalone motor via e. g. a membrane coupling (Fig. 1), instead of using a gear box as connection to a conventional motor. That is a simple solution especially for retrofit designs at a moderate engineering cost. Depending on the particular requirements of the plant, AMBs may are optional here from the rotor dynamics point of view. Unless an oil- and maintenance–free operation is required, lubricated tilting–pad bearings can be sufficient and the more affordable choice. That changes for the second option, where motor and compressor form a unit and share the same housing and bearings, which are in direct contact with the possibly acidic process gas, a potential problem for lubricated bearings. The rotor also becomes longer and rotor dynamics more challenging, whereas in many cases only AMBs allow for a desirable subcritical operation over the entire speed range. While the latter option will be superior in almost any aspect (footprint, efficiency, cooling, power utilization, reliability etc.), the engineering required is tremendous in comparison and therefore reserves the approach for most challenging projects (e. g. subsea oil & gas plants) or products in higher volume production (e. g. industrial heat pumps or turbo blowers).

For highly integrated compressor–motor solutions the motor manufacturer can serve as an engineering partner and provide active parts of the motor. However, the concept and design of the AMBs as well as rotor dynamics lie within the responsibility of the OEM, e. g. the compressor manufacturer. The standalone concept is naturally within the scope of a classical motor manufacturer, like in our case (Fig. 1b). Here, the magnetics bearings are usually considered as part of the product and therefore the motor manufacturers responsibility, which lead to the prototype presented in this paper.

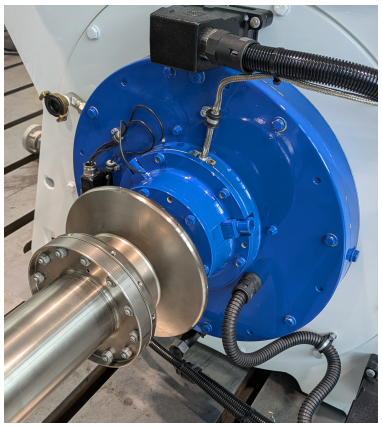

Figure 2 AMB bearing cassette with backup bearings, pressurized–air cooling

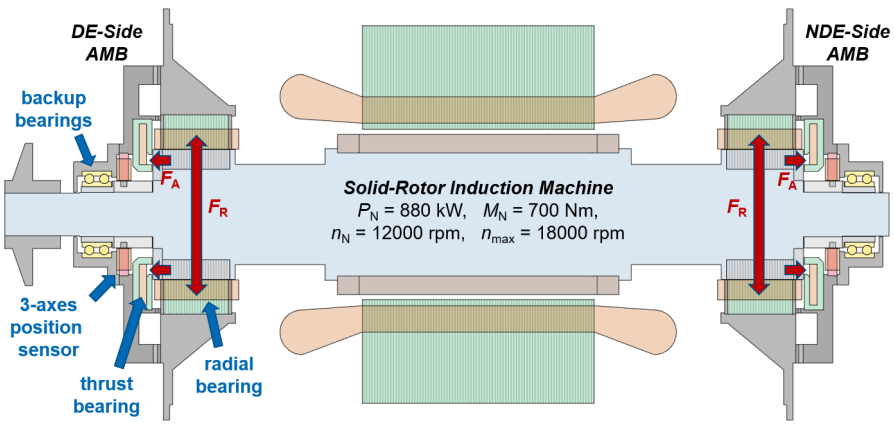

Figure 3 Design concept for rotor and active magnetic bearings with two identical AMB cassettes for simple assembly, including splitted thrust bearing, solid–rotor induction motor

Our goal was to keep the transition from sleeve bearings to AMBs as simple as possible, with two identical bearing cassettes as shown in Fig. 2, enabling the rotor to be assembled in the same way as with mechanical bearings. The final AMB concept is illustrated in Fig. 3. It becomes apparent that the absence of a thrust disk and splitting of the thrust bearing makes the axial force control susceptible to rotor elongation due to heating up of the rotor under load, which needs to be compensated by adapting gains in the controller. Axial air gaps are naturally larger in this case, which we consider uncritical as the axial forces are usually absorbed by the load machine. The 3–axis position sensors from SpinDrive next to the thrust bearings on each drive end have a sensitivity of 7.2 mV/µm and 1.3 mV/µm for radial and axial directions at a resolution of 0.4 µm and 2.4 µm, respectively. They can also replace the commonly required and costly proximity sensors. As backup bearings we utilize two pairs of preloaded double–row angular contact ball bearings with ceramic balls.

3. Design of radial and thrust bearings

The main design goal for the radial bearings was to maximize the force density to allow for a compact geometry similar to the previously used sleeve bearings while providing a sufficiently high force of at least 6.2 kN per bearing. That equals a security factor of $k_F = 4$ in respect to the gravitational force:

$$F_R = k_F \cdot g \cdot \frac{m_{rotor}}{2} \qquad (1)$$

with g describing the gravitation. In general the levers in respect to the gravity center and the according area moments of inertia should also be considered. However, due to the symmetrical arrangement of the bearings and a dominant mass concentration around the gravity center, the simplified estimate in Eq. (1) is adequate. According to Kurvinen et al. (2021) k_F lies commonly in the range 4 . . . 8, where the lower end is usually sufficient for compact and well–studied rotors with moderate unbalances (ref. to e. g. Di et al. (2018)).

As homopolar bearings have an inferior force density (but superior losses) compared to heteropolar bearings and also negatively impact rotor dynamics due their greater length, the latter are the obvious choice here. Especially the works at Lappeenranta University focusing on magnetic bearings for turbomachinery have shown that an E–core design, especially with flux barriers in–between the poles, offer a significantly higher force capacity (about 30 %, Kurvinen et al., 2021) than the classical, most common C–core design (Meeker et al., 1996, Uzhegov et al., 2017). That is why we adapted the 16–pole/12–coil geometry from Jastrzebski et al. (2021). Due to the additional middle tooth compared to the C–core design, it allows for a better utilization of the stator yoke and a higher fill factor in the slots. For more details about the electromagnetic design aspects we refer to the various works of Kurvinen et al. and Jastrzebski et al. Our bearing characteristics are shown in Tab. 1.

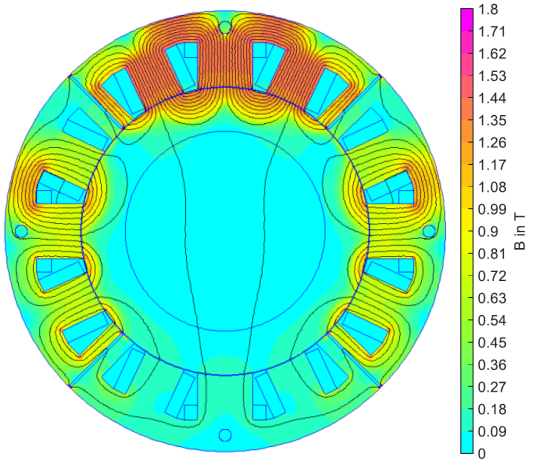

Figure 4 Magnetic circuit of 16–pole/12–coil heteropolar radial bearing with flux–barriers, bias current in all axes and nominal control current in y–axis, nonlinear magnetostatic FE–analysis with FEMM

Table 1 General parameters of radial and thrust bearings

Parameter	Symbol	Unit	Radial Value	Axial Value
Design parameters:				
Rated force (nominal air gap)*	F_{r0}	N	6530	1440
Force at max. displacement*	F_{xmax}	N	4750	760
Number of windings	N	–	60 | 20 | 60	160
Rotor mass (without coupling)	m_{rot}	kg	332	
Rated Speed	n_r	rpm	12 000	
Maximum Speed	n_{max}	rpm	18 000	
Control parameters:				
Natural stiffness*	k_x	N/µm	12.7	1.1
Air gap	g	µm	500	1400
Clearance	c	µm	300	1100
Main inductance*	L_h	mH	48.7	97.5
Coil resistance	R_{cu}	Ω	0.28	0.7
Rated (Bias) Current	I_r	A	13 (6)	13 (6)

*determined by FEA

3.1. Radial bearings: similarities to electrical machines and manufactural restrictions

As we are no manufacturer for AMBs but electrical high–voltage machines, we were seeking similarities to existing recurring motor designs and constructional solutions, which can be transferred to the design and manufacturing of magnetic bearings to finally reduce work and cost. As strikingly comparable in design and capacity, we identified rotating exciters for synchronous machines in e. g. mining trucks, which also use concentrated windings and are similar in size and shape. The principal difference in case of the optimized E–core design are the irregular pole width and coils as well as the additional flux barriers in the stator. The general dimensions of the radial AMBs are described Tab. 2.

The flux barriers constrain the magnetic field of a single pole group to an angle of $-45° \ldots 45°$ in respect to its axis, so that the radial force along the axis is maximized (up to 7 % additional force compared to variant with no barriers). Besides, the axes are better decoupled, as the perpendicular force components of each axis are minimized which leads to a less disturbed control or a possibly simpler controller. To effectively decouple the poles, the remaining iron links between the poles must saturate, so ideally the width of the links should not exceed $0.5 \ldots 1$ mm. However, in case of magnetic bearing stators untypical, our sheet stack is hold together with bolts instead of using a resin–based bonding varnish. Besides that, the tolerances from the stacking process required additional turning of the inner and outer surface, which revealed that slim iron links are unfeasible, as the entire stator would deform. Consequently, unless the manufacturing and stacking of the stator core is mastered with highest precision, the width of the iron links must be increased. Tab. 3, which was determined by nonlinear FE–analysis shows that a combined width of the inner and outer link of 6 mm is an acceptable compromise, where the ratio is determined by mechanical constraints. The inner barriers have a larger impact, though. We have chosen 3 + 3 mm (radial force +5.3 %), while Kurvinen et al. (2021) opted for an unequal ratio.

When it comes to high–speed drives the choice of rotor materials —- especially the sheet material of the AMB rotor — is critical. Its yield strength limits the outer rotor diameter and is therefore decisive for the force capacity of the bearing for a given length and speed, which in turn have to be accommodated with rotor dynamics. Fortunately, a higher yield strength usually is attended with lower losses, which is an advantageous synergy. The in turn lower saturation flux density is less of an issue. On the other hand, the requirements for the stator are contrary: low losses are less relevant due the dominant DC bias fields, but high saturation allows for a higher utilization. That is why we used an automotive–grade NO35–27HS steel sheet in the rotor and a M270–50A sheet in the stator. A cost–saving harmonization of both sheet materials can be considered in less demanding applications.

Table 2 Geometry of radial bearings

Parameter [mm]	Symbol	Value
Outer stator diameter	d_{so}	322
Outer rotor diameter	d_{ro}	210
Shaft diameter	d_{sh}	139
Tooth widths	b_t	22.2…40.2
Stack length stator	l_s	105
Stack length rotor	l_s	109
Stator material		M270–50A
Rotor material		NO35–27HS

Table 3 FEA-study on flux barriers

link width [mm] inside	outside	Σ	Force [N] absolute	increase
Ref.: no barrier			6201	—
20	5	25	6280	1.3 %
10	3	13	6358	2.5 %
5	5	10	6335	2.2 %
4	4	8	6432	3.7 %
2	5	7	6485	4.6 %
4	2	6	6525	5.2 %
3	**3**	**6**	**6533**	**5.4 %**
2	4	6	6536	5.4 %
1	5	6	6539	5.4 %
2	2	4	6613	6.6 %
1	1	4	6650	7.2 %

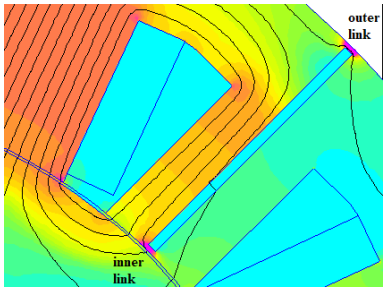

3.2. Thrust bearing

In a turbomachinery drivetrain the fixed bearing carrying the axial load is commonly part of the compressor. Therefore, the forces in the magnetic thrust bearing of the motor are low, at most compensating electromagnetic eccentricities. That allows to forgo the thrust disk, split the bearing and move the halves to both drive ends (compare Fig. 3). The bearing assembly group can be mirrored and the mounting is as simple as for conventional bearings. However, the air gaps must be increased to permit the rotor to elongate under load. Two independent axial position sensors measure the elongation and capacitate the controller to adjust gains accordingly. As dynamic axial forces do not occur in our use case, the design follows standard textbooks. Nevertheless, it is highly advisable to mitigate the impact of eddy currents to achieve acceptable stability margins. Jastrzebski et al. (2021) slitted the stator, which is very effective and allows to use conventional steel like S355J2. To spare the elaborate slitting manufacturing process, we implemented the advice in Seifert (2022) and utilized the stainless steel X20Cr13 for the stator, which has superior soft magnetic properties with $\mu_r = 950$, but a desired poor electrical conductivity of $\kappa = 1.68\,\mathrm{MS/m}$. It is important to note that most stainless steel grades must be soft annealed (+A) to maintain these favorable properties. However, in this state the yield strength usually is indeterminate and not guaranteed by suppliers, which poses an avoidable risk at higher speeds. That is why, for the rotor, we opted for the quenched and tempered 34CrNiMo6+QT ($\mu_r = 194$, $\kappa = 5.26\,\mathrm{MS/m}$) as a compromise between mechanical and soft magnetic properties. The resulting geometry and bearing characteristics are summarized in Tab. 4 and Tab. 1, respectively.

Table 4 Geometry of thrust bearings

Parameter [mm]	Symbol	Value
Stator width	b_s	30.9
Outer stator diameter	d_{so}	308.4
Outer rotor diameter	d_{ro}	210
Active inner diameter	d_i	139
Coil width	b_{cu}	12.2
Coil height	h_{cu}	66.1
Stator material		X20Cr13+A
Rotor material		34CrNiMo6+QT

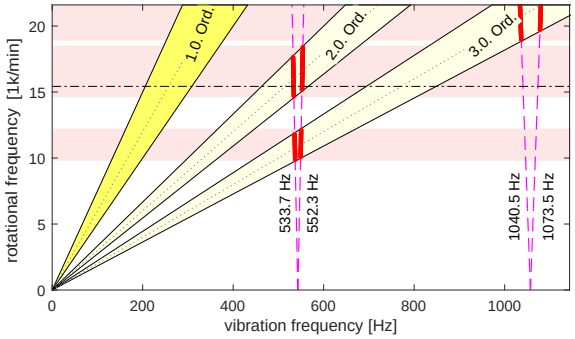

Figure 5 Theoretical Campbell–diagram: 1st and 2nd bending modes, AMBs modeled with linearized parameters, including gyroscopic effect

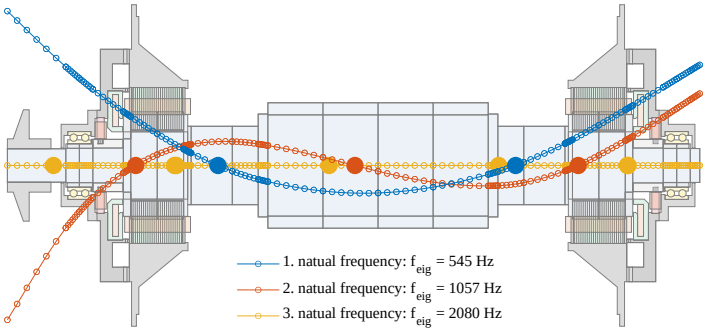

Figure 6 Mode shapes and nodes for 1st to 3rd bending mode in simplified rotor dynamics model based on Timoshenko beam model, AMBs modeled with linearized stiffness and damping under static conditions

3.3. Design aspects related to rotor dynamics

The analysis of rotor dynamics is a crucial aspect in the design process of any electrical drive starting with speeds as low as 1500 rpm depending on its size. High–speed drives with sleeve bearings are almost certainly operated supercritical, where a variety of modes may attribute to this criterion. With AMBs the critical speeds are usually determined unambiguously by the 1st bending mode, which has a comparatively high corresponding eigenfrequency, due to the AMBs' naturally low stiffness essentially leading to a free–free suspension. Crossing of the critical speed with a levitated rotor is very challenging, why usually the rotor design aims for the capacity of subcritical operation. With the compact and symmetric design in our case, we neither expected nor experienced any serious issues. The 1st theoretical bending mode around 545 Hz is sufficiently high and resembles the worst–case, since the slotted motor part of the rotor as well as the rotor lamination of the AMBs were modeled in a simplified manner as additional masses without stiffness. The real bending modes will be higher, which is in accordance with the measured Campbell–diagram in Fig. 11, where we were also able to observe the resonance of the 1st bending mode with a 3rd order excitation as depicted in the theoretical Campbell–diagram in Fig. 5. It is caused by the delta connection of the motor driving 3rd order currents and torque harmonics, but it can be effectively damped by the bearing controller. The nodes of the bending modes (especially the 1st), must lie outside of the sensor and bearing planes, to allow a reliable operation of the bearing. Fig. 6 shows that the condition is fulfilled for the nodes of the first two eigenfrequencies, the 3rd eigenfrequency above 1100 Hz is too high to have an impact.

3.4. Design aspects related to manufacturing

To improve rotor dynamics, high–speed drives in general are usually designed as short as possible and to fully utilize the maximum circumferential speeds dictated by the chosen materials. In Sec. 3.1 and Sec. 3.2 we already discussed the importance of mechanical properties like yield strength for this very choice of materials. They also highly influence the dimensioning and tolerancing of unavoidable radial interfaces between different rotor parts, where the joinability of the parts conflicts with the decreasing interference fit at the desired maximum speeds. To avoid loose parts and guarantee tight fits at any time, tolerances must be chosen wisely. Usually, the temperature difference between parts during the shrink fit must be maximized by cooling down the shaft and the time for the fitting process has to be kept minimal, which requires a controlled and well established workflow.

A specialty of magnetic bearings compared to electrical motors are the very small air gaps and backup bearing clearances of 500 µm and <300 µm, respectively. We found that radial clearances as small as 150…200 µm are feasible and will be aimed for in future projects. Axially, we profit from our experience in classical electrical machine construction, where the use of shim rings is considered during the entire design process, which allows us to exactly adjust all axial gaps.

4. Controller Synthesis and Commissioning

In the following, we will describe the commissioning process and the controller synthesis. We discuss the expectations and difficulties that arise by employing magnetic bearings into our common motor assembly chain and type test procedures. In addition, we will evaluate the overall stability and performance of the model-based SpinDrive Magma® AMB controller operating on our prototype over the entire speed range.

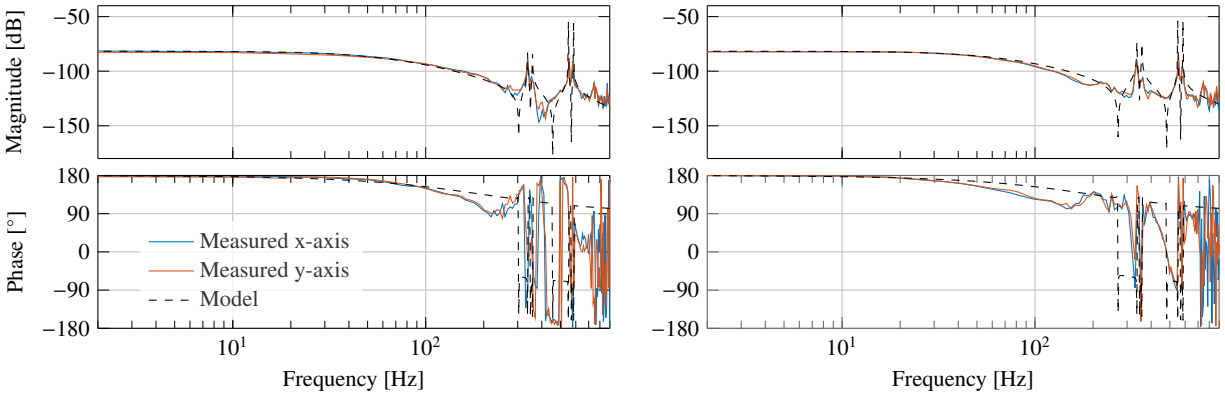

Figure 8 Frequency response of the plant and corresponding model at 15 000 rpm. Left – D-end, right – ND-end.

The levitating rotor was characterized using a stepped–sine excitation approach, in which an input signal was applied to the control input while the corresponding output signals were recorded for analysis. This identification procedure was conducted across a range of rotational speeds in order to account for gyroscopic effects, which significantly influence rotor dynamics at higher speeds. The collected frequency response data enabled a detailed analysis of the rotor–bearing system, facilitating the adjustment of key model parameters such as stiffness and damping. Special attention was given to tuning the frequencies of the bending modes, which are critical for accurately capturing the dynamic behavior of the rotor. Based on the identification, two eigenfrequencies at approximately 347 Hz and 567 Hz were determined. The latter characterizes the first bending mode of the rotor following the findings in Sec. 3.3. The former describes the rotation of the housing around its vertical axis and will be excluded in the next iteration of the controller synthesis.

An illustrative example of the identification results at a rotational speed of 15 000 rpm is provided in Fig. 8, demonstrating a close match between the measured system response and the fitted model. This validated model captures both the structural dynamics and the gyroscopic behavior of the system with sufficient fidelity, making it a reliable foundation for subsequent control system development. In particular, it serves as the basis for the design of a model–based controller aimed at improving rotor stability and performance during operation. The accurate dynamic representation obtained through this process ensures that the controller can effectively account for the complex interactions inherent in the levitating rotor system.

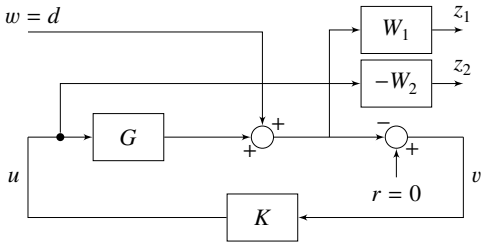

Figure 7 S/KS mixed-sensitivity problem in standard form

For stabilizing the position controller, the model–based $\mathcal{H}_\infty$ controller was used in its mixed sensitivity form as presented in Fig. 7, similar to the one described by Uzhegov et al., 2023. The main benefit of such an approach is a relatively straightforward tuning process, where — based on the identification data — few parameters of the plant model have to be corrected. For this particular problem, the following weights have been selected:

$$W_s = \frac{0.4s + 17.28}{s + 0.1728} \quad \text{and} \quad W_{KS} = \frac{10s^3 + 5.496 \cdot 10^4 s^2 + 1.511 \cdot 10^8 s + 2.076 \cdot 10^{11}}{s^3 + 2.755 \cdot 10^4 s^2 + 3.794 \cdot 10^8 s + 2.613 \cdot 10^{12}} \tag{2}$$

Besides the stabilizing position controller to counteract the residual unbalance, the generalized notch filter is used. The implementation is based on the work of Herzog et al., 1996, where filter extracts synchronous part from the sensor signal. In that way the saturation of actuator voltage along with vibrations is avoided at the cost of letting the rotor oscillate slightly in the available air gap.

The rotor orbits are shown in Fig. 9, where it is evident that after applying synchronous filtering, only approximately 10 µm of residual motion remains, which can be attributed to noise. This residual displacement is relatively small, indicating effective suppression of dominant disturbances. A detailed examination of the frequency spectrum in Fig. 10 reveals that the primary contributor to the residual noise is a third-order harmonic. This component is likely caused by surface runout on the rotor, which introduces periodic disturbances at integer multiples of the rotational frequency. Another plausible source of this harmonic is the current and torque ripple originating from the electrical motor. The motor in question employs a delta-connected winding configuration, which can exacerbate harmonic content in the stator currents and, consequently, in the torque output.

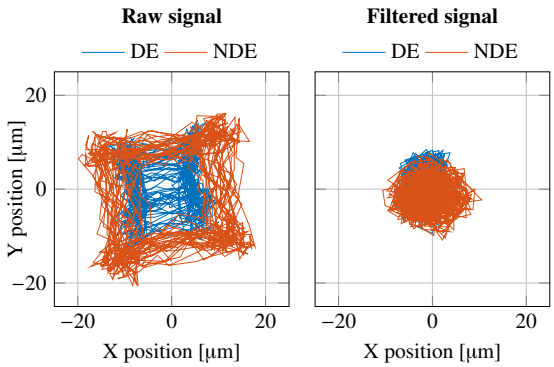

Figure 9 Orbits of the rotor ends at 15 000 rpm. Left – the raw values from the sensors. Right – the input data for the controller after filtering.

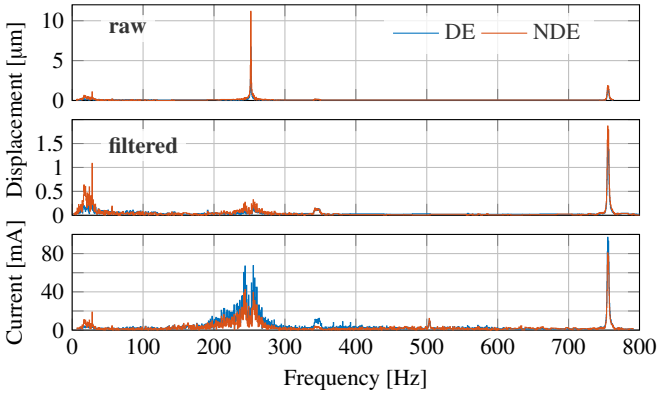

Figure 10 Spectrums of raw sensor measurements (top), sensor signal after filtering (middle) and control currents for radial bearings (bottom)

Mitigating the third-order harmonic is particularly important, as its interaction with the rotor's flexible modes could amplify vibration amplitudes if left unaddressed. Therefore, targeted filtering of this harmonic is beneficial for maintaining rotor stability, especially when operating near critical speeds. In addition to the third-order component, the control current also shows energy concentrated in sidebands around the 1st–order synchronous harmonic. These sidebands are attributed to slight variations in rotational speed and sensor noise, which cause the narrowband notch filter to allow some leakage. Although the filter is designed to be highly selective, its narrow bandwidth means that even minor frequency shifts can result in incomplete suppression of sideband frequencies. Addressing these residual components through adaptive filtering or speed–synchronized techniques, also for higher excitation orders, may further improve system performance and reduce control effort. At the current state, we only focused on the synchronous harmonic.

5. Evaluation of Experimental Data

In this section we evaluate the experimental vibration data in the form of the exemplary Campbell–diagram in Fig. 11 (NDE, horiz.) and link it to the findings of Sec. 3.3 and Sec. 4. For further quantitative illustration, Fig. 12 shows slices of the Campbell–diagram alongside the excitation lines. The data shown here results from the initial commissioning of the AMBs and can be considered preliminary, leaving room for improvement by iteratively fine–tuning the controller based on the findings in this article.

First of all, it is important to distinguish between excitations and eigenfrequencies which actually are related to the rotor and should be considered by the AMB controller. On the other hand, oscillations of the housing only, are preferably decoupled from the rotor – which poses the major challenge for our configuration. That is because the stiffness of the housing is comparatively low, showing known significant modes at 41 Hz, around 190 Hz and 250 Hz and at 347 Hz. The latter is especially responsive to an excitation by the AMBs (cf. Fig. 8), but less of an issue, as it lies outside of the radial AMBs' bandwidth of roughly 200 Hz (-3 dB). It becomes apparent, that within this broad bandwidth all housing modes are equally excited over all speeds. We learn, that the housing should be stiffened such that most of its modes are shifted

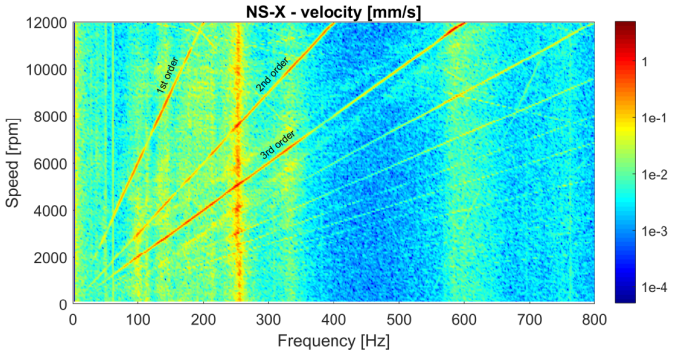

Figure 11 Campbell–diagram measured at NDE bearing shield, X–direction

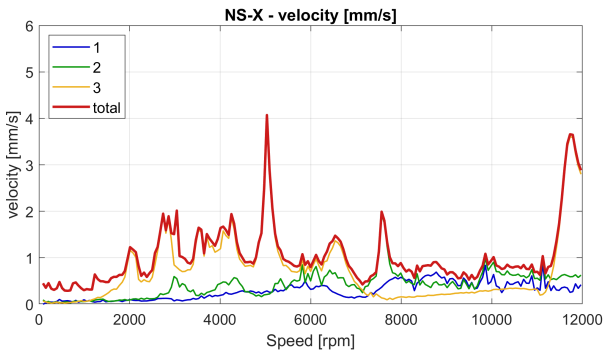

Figure 12 Slices of Campbell–diagram along excitation lines, total vibration velocities (NDE–X)

outside of the AMBs' bandwidth. For the current setup we aim to adapt the controller, such that at least the apparent resonance at 250 Hz is mitigated.

Apart from the broadband excitation by the AMBs we have particular excitations by the motor. The 1st–order excitation is the actual rotation of the rotor, which can be effectively filtered from the position signal and does not significantly contribute to the measured vibrations (<1 mm/s as shown in Fig. 12). The 3rd–order has a major impact on the overall vibration amplitudes. Also, it obviously reacts with the first bending mode of the rotor at 12 000 rpm, which implies that the delta–connection of the stator also mechanically effects the rotor. The 2nd–order excitation, purely stator–related (2–pole motor), has less impact, apart from its interaction with the housing mode at 250 Hz.

From the currently available data we are not able to conclude, whether the AMBs amplify these particular speed-related excitations or not. But as the first bending mode at 567 Hz is far greater than the bandwidth of the AMBs, an additional speed–adaptive filtering of the 2nd and 3rd–order excitations may be possible and helpful.

6. Summary and conclusion

In this article we presented a well–working prototype of a 1 MW high–speed motor with levitating rotor. While the concept, design and manufacturing of the AMBs was done in–house at VEM, the sensors and bearing controller was provided by SpinDrive. We elaborated on the choice of materials and physical boundaries they imply. Furthermore, we identified recurring designs and constructional as well as technological solutions which can be transferred from electrical motors to the design and manufacturing of magnetic bearings. As a result, we adapted a proven 16-pole/12-coil design for the radial AMBs and studied the impact of the flux-barriers at the empty poles separating the coil groups.

In experiments, we proofed that the motor runs without any instabilities up to at least 15 000 rpm with mostly reasonable low vibrations over the entire speed range, which was only limited by the available motor inverter. However, we still see a significant improvement potential both for the current prototype as well as for future projects. The bearing controller can be optimized to address the peculiarities of the motor more effectively. On the one hand, the applied notch filter for the 1st–order excitation may be speed–adaptively extended to the 2nd and 3rd–order to avoid further amplification of resonances, imposed by the low eigenfrequencies of the housing. On the other hand, the most significant resonance at 250 Hz may can be spared from AMB control. Compared to passive mechanical bearings, the actively controlled magnetic bearings add additional actuators to the overall system, causing excitations we have not been familiar with. As a consequence, we learned that a modal analysis of the housing is of increased importance and future constructional designs of our housings will be improved (e. g. stiffened) to allow for an effective decoupling from the excitations evoked by the magnetic bearings. In the following, after optimization of the latest prototype and further data acquisition, we will conduct a comparative study of the sleeve and magnetic bearings of our otherwise similar prototype motors — in terms of rotor dynamics, practicality and economic aspects.

References

Di, C. et al. (2018). "Unbalanced Magnetic Pull Compensation With Active Magnetic Bearings in a 2 MW High-Speed Induction Machine by FEM". In: *IEEE Transactions on Magnetics* 54.8, pp. 1–13.

Durantay, L. et al. (2023). "Variable Speed Direct Drive Induction Motors Levitated by Active Magnetic Bearings for Oil and Gas Compression Services". In: *18th International Symposium on Magnetic Bearings*.

Herzog, R. et al. (1996). "Unbalance compensation using generalized notch filters in the multivariable feedback of magnetic bearings". In: *IEEE Transactions on Control Systems Technology* 4 (5), pp. 580–586.

Jastrzebski, R. P. et al. (2021). "Design and Modeling of 2 MW AMB Rotor With Three Radial Bearing-Sensor Planes". In: *IEEE Transactions on Industry Applications* 57.6, pp. 6892–6902.

Kurvinen, E. et al. (2021). "Design and Manufacturing of a Modular Low-Voltage Multimegawatt High-Speed Solid-Rotor Induction Motor". In: *IEEE Transactions on Industry Applications* 57.6, pp. 6903–6912.

Meeker, D. C. et al. (1996). "An augmented circuit model for magnetic bearings including eddy currents, fringing, and leakage". In: *IEEE Transactions on Magnetics* 32.4, pp. 3219–3227.

Seifert, R. (2022). "Fraktionale Flussdichteschätzung in aktiven Magnetlagern". PhD thesis. TU Dresden.

Uzhegov, N. et al. (2017). "Design Aspects of High-Speed Electrical Machines With Active Magnetic Bearings for Compressor Applications". In: *IEEE Transactions on Industrial Electronics* 64.11, pp. 8427–8436.

Uzhegov, N. et al. (2023). "Control and Commissioning of Active Magnetic Bearing (AMB) System for High-speed 1 MW Turbo Blower". In: *18th International Symposium on Magnetic Bearings*. Lyon, France.